ASME Journal of Micro- and Nano-Manufacturing
Online journal at:
https://asmedigitalcollection.asme.org/micronanomanufacturing

Md Ibrahim Khalil
Department of Mechanical Engineering,
University of Maine,
Orono, ME 04473

Md. Akibul Islam
Department of Mechanical Engineering,
University of Maine,
Orono, ME 04469

Dezhong Tong
Department of Mechanical and
Aerospace Engineering,
University of California, Los Angeles,
Los Angeles, CA 90025

Mohammad Khalid Jawed
Department of Mechanical and
Aerospace Engineering,
University of California, Los Angeles,
Los Angeles, CA 90095

Bashir Khoda[1]
Department of Mechanical Engineering,
University of Maine,
Orono, ME 04473

Controlling Surface of Rods With Entrained Particle as Asperities

Changing the surface properties (i.e., roughness or friction) can be instrumental for many applications but can be a complex and resource-intensive process. In this paper, we demonstrate a novel process of controlling the friction of a continuous rod by delivering inorganic microparticles. A standardized continuous particle transfer protocol has been developed in our laboratory for depositing particles from a liquid carrier system (LCS) to the cylindrical rod substrate. The particle transfer process can produce controllable and tunable surface properties. Polymeric binder is used to deliver the particles as asperities over the rod substrate and by controlling their size, shape, and distribution, the coefficient of friction of the rod is determined. Tabletop experiments are designed and performed to measure the friction coefficient following the Capstan equation. The entrained particles on the substrate will create size- and shape-based asperities, which will alter the surface morphology toward the desired direction. Both oblique and direct quantitative measurements are performed at different particles and binder concentrations. A systematic variation in the friction coefficient is observed and reported in the result section. It is observed from the capstan experiment that adding only 1% irregular shaped particles in the suspension changes the friction coefficient of the rods by almost 115%. The proposed friction control technique is a simple scale-up, low-cost, low-waste, and low-energy manufacturing method for controlling the surface morphology. [DOI: 10.1115/1.4064646]

Keywords: micro-particle, friction coefficient, capstan equation, particle entrainment

1 Introduction

Rods are one-dimensional structures that have several advantages compared to other forms of materials (i.e., powder, sheet, or liquid). Elastic rods find applications in various aspects of daily life, serving purposes such as sailing, climbing, and various industrial uses. The control of friction on these rods plays a crucial role in achieving better control over their applications. Manipulating the friction of the rod can be accomplished by depositing and adhering particles onto its surface. The method of particle delivery depends on the specific operating conditions, which is a manufacturing process with considerable parameters. Among the techniques employed for particle transfer, physical vapor deposition [1,2], chemical vapor deposition [3,4], and plasma sputtering [5,6] are utilized to create a uniform thin metallic layer under high vacuum conditions. However, these processes tend to be slow and resource-intensive when applied in industrial settings. Conversely, wet deposition-based sol–gel coating techniques offer a fast and cost-effective alternative, as they can be conducted under atmospheric conditions using an evaporating solvent or media [7–9].

Considerable research has been conducted on wet deposition-based dip coating, with a particular focus on the transfer of materials either from suspension (direct transfer) or from precursor chemicals (ionic transfer). This process is capable of accommodating a wide range of solution densities and viscosities during the film formation process, making it suitable for coating cylindrical and flat substrates [10]. In the dip coating process, material is deposited onto the surface of the substrate as it is withdrawn from the suspension [11]. This technique is widely employed due to its simplicity, affordability, and the ability to control film thickness. The thickness of the polymer layer on the substrate is determined by the competition between capillary force and viscous drag force during the withdrawal process [12,13]. The film thickness can range from nanometers to a few microns and is the function of the fluid and substrate characteristics as well as the process parameters. This film formation method finds extensive usage in diverse industrial applications, including corrosion protective layers [14,15], biosensors [16], orthodontic wires [17], and anti-icing surfaces [18], among others. By incorporating immiscible inorganic fillers, nanoparticles, or clusters into the solution, the coating process can become an effective particle transfer process [19,20]. The precursor solution, often called a LCS, can carry the particles and deliver them on substrate or in structures at a substantial rate.

The LCS-based particle transfer process often contains positively or neutrally buoyant immiscible nanoparticles to make the homogeneous mixture [21]. The property (i.e., viscosity) of the LCS is often tailored to match the specific density of the particle while maintaining a dilute or Newtonian regime. Particles are entrained on the substrate, and evaporation of the volatile compound (solvent) leaves a dried film as a coating at the liquid–gas interface. The particle-surface adhesion force can be categorized as

[1]Corresponding author.
Contributed by the Manufacturing Engineering Division of ASME for publication in the Journal of Micro- and Nano-Manufacturing. Manuscript received September 24, 2023; final manuscript received January 24, 2024; published online February 28, 2024. Assoc. Editor: Bruno Azeredo.

(i) electrostatic, (ii) van der Waals, (iii) covalent bond, (iv) hydrogen bond, and (iii) gravitational forces [22–24]. For submicron size particles, the electrostatic force and van der Waals become prominent to adhere to the substrate due to their possession of a large specific surface area. However, larger microparticles ($>1\ \mu$m) are noninteracting and nonagglomerating spherical solid particles in the liquid matrix (non-Brownian regime) [25,26]. Due to the higher liquid-to-specific particle density ratio, the gravitational force on the microparticles dominates the other forces, which differ from LCS-based density-matching particle transfer process. To counter the gravitational force, external kinetic energy in the form of agitation will be applied to create a pressure difference (normal stresses), and the particles will stay suspended, creating a dispersed mixture ("pseudo–suspension"). Additionally, binders can be selected and added to influence interactions through the polymer layer for large particles. The presence of the binder also ensures the sustainable particle transfer with sufficient adhesion force.

The friction within and between the contact surface on a rod determines the functionality of rod applications. The coefficient of friction, rather than being an intrinsic material property, serves as an indicator of the contact state between two bodies and fluctuates with wear. Previous research has predominantly focused on the average value of the friction coefficient rather than the evolution of friction coefficient [27]. Only a few studies have experimentally explored the evolution of friction forces [28]. Understanding and controlling the frictional properties of rods are of significant interest due to their widespread use in various applications. By manipulating the friction forces acting on these rods, it becomes possible to enhance their performance and optimize their usage. In this study, we delve into the effects of particle deposition on rods and its impact on frictional behavior. First, we present a novel continuous particle delivery method for varying the friction force of a rod with adhered particles on the surface along its length. The asperities resulting from particle adherence cause changes in surface morphology, which can be quantified as friction forces. To investigate the relationship between particle characteristics and friction forces, we conducted a series of experiments involving the coating of the rods with suspensions of varying particle size, shapes, and concentrations. The friction coefficient of the coated rods is measured using the capstan equation, and a systematic variation of friction can be observed which are presented in the result and discussion section. The proposed friction control technique is a simple to scale-up, low-cost, low-waste, and low energy manufacturing method for controlling the surface morphology.

2 Experimental Details

In this section, the details of the different stages of the experimental process are described. For the experiment, we prepared the elastic rods and the LCS for particle delivery on the rods first. The particle delivery setup and the friction force measurement setup are described in the following section.

2.1 Rod Substrate and Liquid Carrier System Preparation. We used natural rubber rods (procured from McMaster-Carr Inc., USA) as substrate in the experiment. The diameter of the rods used is 1.59 mm. The Young modulus is measured in the lab using the universal testing machine (MTS criterion, USA) as 1.83 MPa and the manufacturer suggested working temperature range is $-59\ ^\circ$C to $122\ ^\circ$C. The surface of the rubber rod is relatively smooth, and the average roughness is measured as 0.8 μm using VHX 7000 Digital 4 K microscope (KEYENCE Corp., IL). Asperities are introduced by delivering metal particles over the rods to control the surface property and systematically varying the friction coefficient. Iron metal reduced irregular-shaped powder (particles size 45–150 μm, Chem Center LLC, CA) and nickel-based eutectic alloy spherical powder (particles size 0–20 μm, NicroBraz LM, OH) are considered to create the asperities on the rod's surface.

To achieve the uniform deposition of particles, an LCS is prepared in the laboratory. The LCS consists of binder (polymethyl methacrylate; MW$\sim$15,000 g/mol; procured from Sigma Aldrich, USA) and solvent (1,3-Dioxolane). The density of the binder and solvent is 1.19 g/cm^3 and 1.06 g/cm^3, respectively. The wettability between LCS and the natural rubber rods has been observed and considered sufficient. Two different shapes of particles are added to the LCS to prepare the suspension as shown in Fig. 1. The addition of binder in the solution will increase the viscosity that will increase the capillary number and the binder film thickness on the substrate after dipping. Increased amount of binder will also facilitate the adherence of particles over the substrate. The volume fraction of the binder and particles in suspension is kept within 13% to ensure dilute regime. The viscosity and the shear stress of the LCS with 1–7% (w/v) binder polymer are measured using an Anton Paar MCR 302 Rheometer with a 50 mm parallel plate geometry as shown in Fig. 2. Our findings revealed a systematic variation in both viscosity and shear stress as the binder's concentration increases. The viscosity remains mostly flat with the binder concentration range used, which demonstrates their Newtonian behavior.

2.2 Continuous Particle Delivery Setup. The elastic rods are coated in a custom-made continuous particle transfer setup developed in our laboratory. The schematic diagram and the experimental image are shown in Fig. 3. Minimum suspending speed is provided for agitation with straight blade impeller (Fig. 3(*b*)) to create a pseudo-suspension for particle delivery via entrainment. The minimum suspending speed for the impeller will reduce the vortex in the complex mixture and help toward the

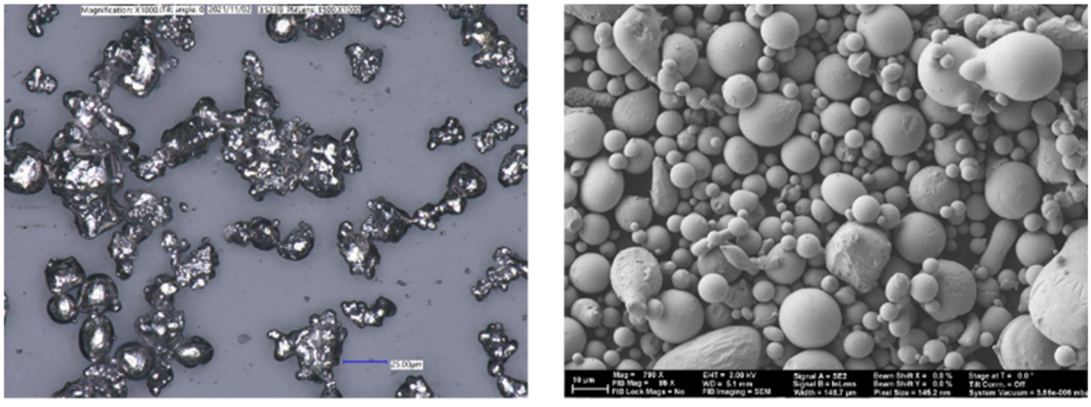

(*a*) (*b*)

Fig. 1 Morphology of the particles: (*a*) irregular shaped reduced iron metal particles and (*b*) spherical nicrobraz 51 particles

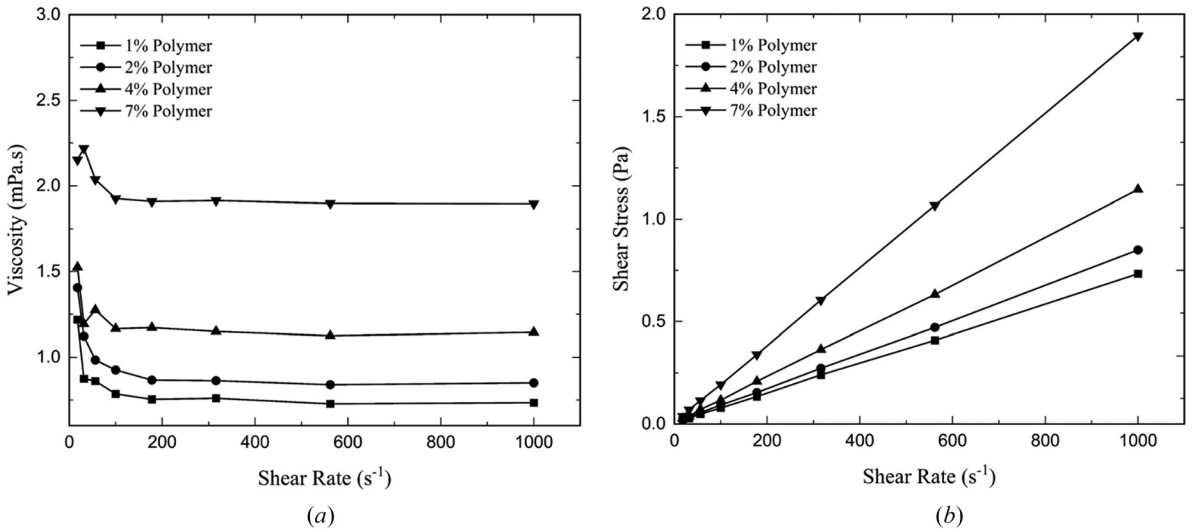

Fig. 2 Rheology of the liquid carrier system (LCS): (*a*) variation of the viscosity and (*b*) variation of shear stress with change in shear rate

laminar flow assumption. The continuous particle transfer setup consists of a dipping jar, guiding rollers, an impeller, a motor, and the control box for the motor. A cylindrical screw top and a clear borosilicate glass jar are used as dipping jar. The inner diameter (D_i) and the height (H) of the dipping reactor are 80 mm and 100 mm, respectively. As the density of the particles (7.8 g/cm^3) is much higher than the solution, a straight blade impeller ($W = 12.5$ mm and $L = 70$ mm) is used to keep the particle suspended during the transfer process. The rotation of the impeller creates a pressure difference, which helps the particles to overcome the gravitational effects. The uncoated rod is inserted from one side of the dipping jar (as shown in the schematic) and the rod is guided by three guide rollers ($R1$, $R2$, $R3$). The coated rod is pulled by the motor (M) on the other side of the jar. The withdrawal speed of the rod is kept at 5 mm/s and the dwell time in the suspension is about 10 s. The motion of the rod during the coating process is controlled by a high precision (±2%) stepper motor and the motor is controlled by a Flashcut controller using G-code. To reduce the effects of the solvent and better adhesion of particles during the friction force measurement tests, the coated rods are placed in an oven at 80 °C for 1 h to ensure uniform polymer binder film formation and sustainable adhesion of particles.

2.3 Friction Test Setup. The elastic rod at different coating conditions will have various asperities creating distinct topography, which will result in different frictional characteristics. To capture the surface properties, rods with entrained coated particles and uncoated rods are considered to measure the friction force at self-intersecting conditions, tying an overhand knot. The rods are tied (as shown in Fig. 4) to achieve self-intersection conditions. The friction force is measured using our setup, which is comprised of a rail (400 mm), a push-pull force gauge (±20 N), a bipolar stepper motor, and a Flashcut controller. One end of the rod is kept in the fixed clamp and another end is mounted to the hook of the force gauge. Due to the motion of the force gauge, the friction force at the self-intersection contact is recorded at 10 Hz. The pulling speed of the rod is 200 mm/min.

For quantitative analysis, friction coefficient is directly measured and reported following the capstan equation. An experiment is designed to measure the friction coefficient with sliding motion as

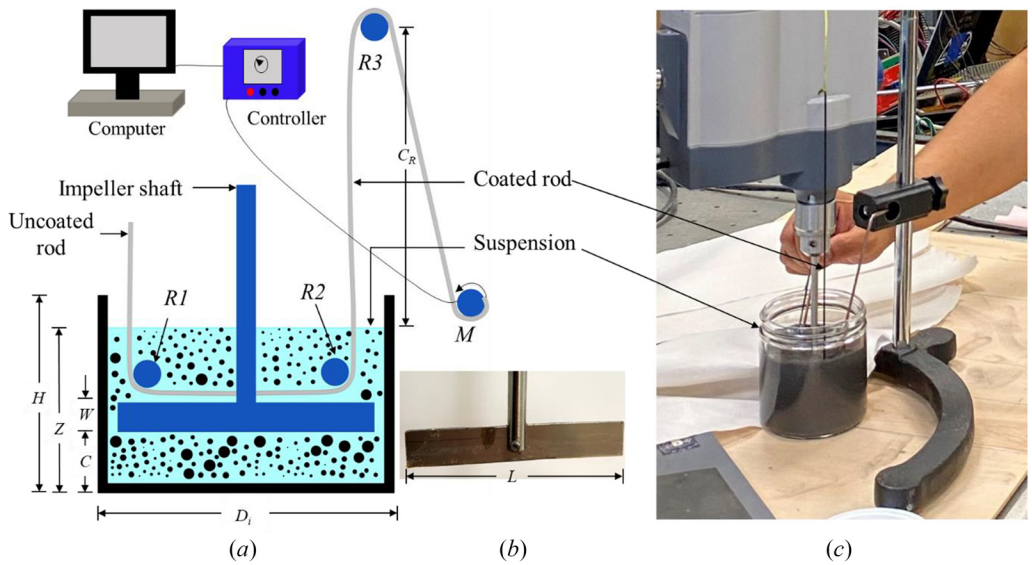

Fig. 3 Continuous particle transfer setup: (*a*) schematic diagram, (*b*) impeller used for LCS agitation, and (*c*) experimental setup (not to scale)

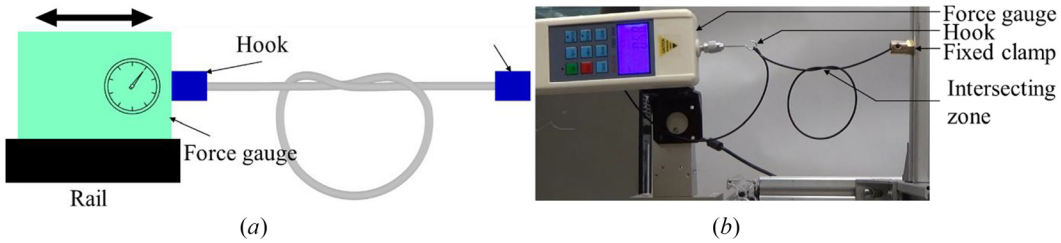

Fig. 4 Comparative force measurement setup: (*a*) schematic and (*b*) experimental

shown in Fig. 5. The capstan equation ($T_2 = T_1 e^{\mu\theta}$), also known as the Euler equation of tension, combines the relation between the maximum load (T_2), minimum load (T_1), contact angle (θ), and coefficient of friction (μ). As the friction coefficient is considered at the self-contact of the rods in our experiment, a larger diameter rod (1/4 inch) of the same material is used as the capstan to measure the friction coefficient. Both the capstan and the sliding rod are coated with the same suspension following the protocol discussed earlier. The schematic diagram and experimental image of the experiment are shown in Figs. 5(*a*) and 5(*b*), respectively. The rod slides over the capstan following the weight difference at two ends and the friction coefficient is calculated. A dead load (T_1) is setup on one end of the rod and a variable load is attached on another end (T_2).

3 Results and Discussion

The result of the friction force experiment with overhand knot and the capstan experiments are discussed in this section. Both oblique and direct quantitative measurements are performed at different binder and particle concentrations. When the rod is inserted into the suspension, a thin polymer layer is formed over the rod at the solid–liquid interface. The thickness of the polymer layer is dependent on the viscosity of the suspension, which is dependent on the volume fraction of the polymer. During the withdrawal of the rod from the suspension, particles are entrained over the rod surface due to the convective flux. The upward convective flux is dependent on the withdrawal speed of the rod and viscous drag force. The thickness of the polymer film for a nonevaporating solution formed over the substrate is often predicted by Landau and Levich and then Derjaguin, which is known as the famous LLD equation [29,30]. The modified LLD equation is used here to calculate the polymer film thickness over fiber using $h = 1.34RCa^{2/3}$ [31,32] and the results are shown in Table 1. As the polymer binder concentration increases in LCS, the polymer layer thickness increases, which helps entraining the larger particles for larger asperities.

A similar polymeric layer of poly methyl methacrylate (PMMA) is formed around the particles with acrylate monomer. When the coated particles come close to the coated substrate in the suspension due to the dispersion energy, an adhesion bond will form between the interfacial polymer films. No direct contact is expected between particles and rod. Besides, due to their non–Brownian size, electrostatic force and van-der Waals force are not prevalent between and within particles. The adhesion of particle on the rod substrate can be a complex interfacial interaction causing physical link through polymer bridging between particle and rod substrate. With PMMA film thickness measured at a couple micrometer thick on the rod substrate, the polymer bridging could be a considerable factor. Additionally, capillary force during the rod retraction can be significant; the PMMA solution bridges the gap creating a capillary pressure that can hold the particles in place. Furthermore, tribological interactions (i.e., friction) can be prominent to counter the gravitational force during rod retrieval, which can facilitate the particle transfer from the mixture. Due to the smooth rod surface ($\boldsymbol{R_a} = 0.96\ \mu m$), and larger particle size (avg dia. 27 μm), geometric and mechanical interlocking of particles on the rod substrate will not be prevalent in this system. The particle adhesion process can be influenced by specific physical process parameters such as the relative motion between the substrate and particles, surface energy, wettability of the substrate, viscosity of the suspension, and particle morphology. The correlation between the particle transfer and process parameters, including the viscosity of the suspension [19], surface energy [33], molecular weight [34], and withdrawal speed

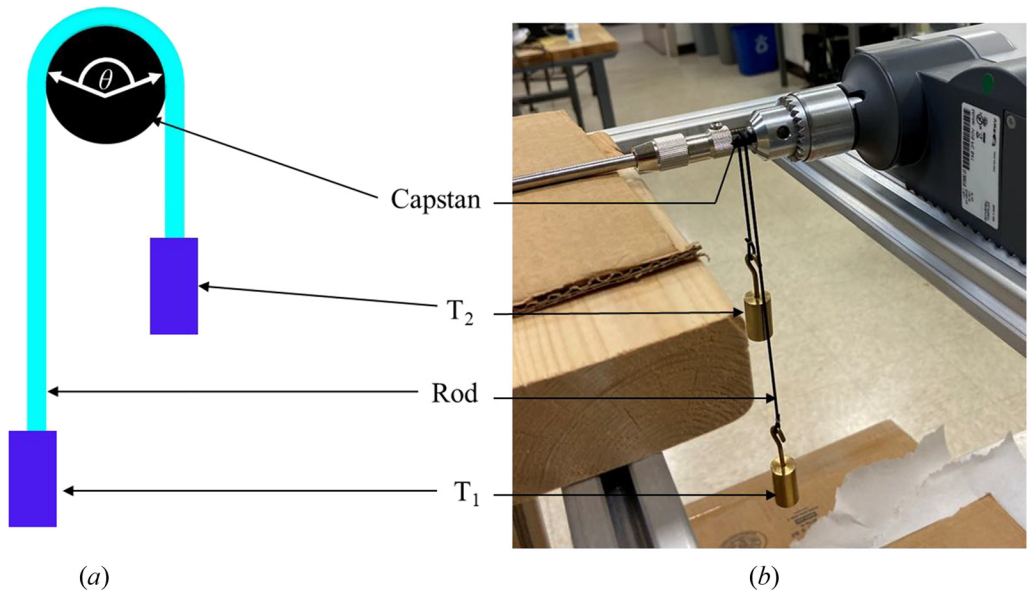

Fig. 5 Capstan experiment setup: (*a*) schematic of the experiment and (*b*) experimental setup. Angle θ denotes the total winding angle.

Table 1 Process characteristics for LCS and polymer layer thickness measurement

Binder concentration (%)	Viscosity of the solution (mPa·s)	Surface tension of the solution (mN/m)	Density of the solution (g/cm^3) × 10^{-2}	Withdrawal speed (mm/s)	Capillary number (10^{-3})	h (μm)
1	0.84	34.37	106	5	0.122	2.62
2	0.98	34.43	106.3	5	0.143	2.91
4	1.22	34.57	106.6	5	0.176	3.35
7	1.99	34.77	107	5	0.287	4.63

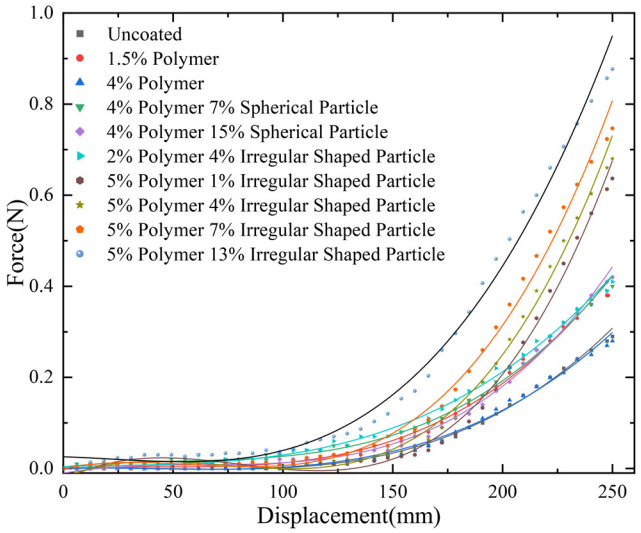

Fig. 6 Variation of friction of elastic rod at different coating conditions

[21,35], has been explored in prior research and is a nontrivial research question.

The strength of the adhesion force and hence the sustainability of the particle transfer is often attributed to the thickness of the polymeric layer. For nanoparticle entrainment, the desired thickness has been reported as the diameter of the particles. In one of the previous articles, Colosqui et al. [36] numerically showed particle diameter should be equal to polymer film to entrain particle in the polymer film. Although, for microparticle entrainment or entrapment, such literature is scarce. Six time large particle entrainment has been reported by Sauret et al. [37]. In one of our previous articles, we demonstrated that the thickness to diameter ratio is 0.16 for high-specific density microparticle transfer [33], which is consistent with the size of entrained particle in this work. For irregular iron particle, the average particle size is measured as 27.16 μm following the protocol described in literature [38], and the polymer film thickness (as indicated in Table 1) followed the 0.16a relationship for their entrainment. Thus, producing larger asperities by entraining irregular microsized larger particles aligns with our previous findings.

The entrained particles on the substrate will create size- and shape-based asperities, which will alter the surface morphology. The force versus displacement plot (Fig. 6) is generated by polynomial (cubic) fitting of the scatter data points collected from the force gauge discussed earlier. The self-intersecting overhand knot exposes the pulling force required to pull the rod, which is an oblique technique for determining the surface morphology variation. While pulling the rod, both tensile and torsional forces will be transmitted to the self-intersecting configuration of the rod because of the topology of the overhand knot. Static friction plays an important role as rods contact each other while pulling the rods. Acting as a threshold force, static friction prevents relative motion between the rods. It maintains the system in a state of static equilibrium, resisting the initiation of movement until an external force surpasses the maximum static friction force. This transition marks the onset of dynamic friction, where the rods either start sliding past each other or continue to resist relative motion. Once this resistance is overcome, the dynamic friction force will come into action. Both size and shape effect of the entrained particles can be observed in the plot with systematic variation. From the experimental results, it is clear (Fig. 6) that the uncoated rod shows the lowest friction force due to the smoothness of the rod (lower roughness number), and no asperities are introduced. The friction of the rods is increased gradually when the rods are coated by the polymer solution only. However, the rod coated with 4% polymer shows lower friction force than the rod coated with 1.5% binder. When the volume fraction of polymer increases in the solution, it induces more polymers over the rod. This reduces the friction instead of increasing it.

Table 2 Data for friction coefficient measurement with capstan experiment

Coating	Trial number	Load T_2 (gm)	Load T_1 (gm)	Total wind angle, θ (rad)	Load ratio (T_2/T_1)	Friction coefficient (μ)	Average friction coefficient
Uncoated	1	47.60	20	π	2.38	0.27	0.25
	2	44.27	20	π	2.21	0.25	
	3	43.55	20	π	2.18	0.24	
1% Particle	1	109	20	π	5.45	0.53	0.55
	2	117	20	π	5.85	0.56	
	3	112.4	20	π	5.62	0.54	
4% Particle	1	140.7	20	π	7.03	0.62	0.62
	2	153	20	π	7.65	0.64	
	3	130	20	π	6.50	0.59	
7% Particle	1	170	20	π	8.50	0.68	0.66
	2	150	20	π	7.50	0.64	
	3	158	20	π	7.90	0.65	
13% Particle	1	255	20	π	12.75	0.81	0.78
	2	221	20	π	11.05	0.76	
	3	233	20	π	11.65	0.78	

In this study, the major difference between the iron and the nickel particles is the shape of the particles. We observed the shape effect of the surface morphology as a response to the friction force with two different types of particles (spherical and irregular shown in Fig. 1). During the coating with spherical particles, we kept the polymer binder volume fraction constant (4%) and varied the particle volume (7% and 15%). The variation of the friction force with the variation of the volume fraction of spherical particles is not observed as significant. At a fixed binder volume fraction, the polymer film thickness remains the same and can only entrain certain size particles [19]. As a result, even with increased particle volume (from 7% to 15%), asperities created by the entrained particles do not change much, which suggests the size effect is not activated in this circumstance. The curvature of the spherical particle is relatively smooth compared to the irregular shaped particles, which results in lesser resistance and lower friction force. In contrast, the contact region of the irregularly shaped particles is higher causing a higher degree of surface roughness and a more intricate interaction at the microscale. They also have potential for interlocking, which may contribute to enhanced overall frictional effects. The roughness of the uncoated rod is measured as $R_a = 0.96\,\mu$m, while the R_a value for 1%, 4%, 7%, and 13% irregular particles are measured as 4.52 μm, 4.32 μm, 10.44 μm, and 15.94 μm, respectively. This indicates a progressive and significant augmentation in surface irregularities as the particle concentration escalates. As a result, with a small amount of polymer (2%) and irregular particle (4%) volume fraction, higher frictional force is observed than the spherical particles, which is the motivation for using the irregular shaped particles at the later analysis.

The collected data from the friction coefficient measurement are shown in Table 2. Due to the shape of particles, the rods coated with irregularly shaped particles increase the friction significantly than the other coating condition, which is observed in Fig. 6. When the rod is dipped in the polymer solution, a viscous layer is formed, which helps to entrain the particles on the surface. The thickness of the viscous layer increases with higher polymer content as shown in Table 1. Since the irregular shaped particles are larger in size than our spherical particles (0–20 μm), a higher polymer content (5%) is applied for the entrainment of those irregular shaped larger particles. We observed a systemic increase in friction force and coefficient with the increase in particle volume fraction. The friction force is maximum when the particle volume fraction is maximum (13%) in the suspension and the friction force is minimum with minimum particle (1%) in the suspension. This is due to the increase in probability of collision between substrate and particles at higher volume fraction. Figure 7 illustrates particle attachment to the rod surface (a, b, c, and d corresponds to particle transfer at concentrations of 1%, 4%, 7%, and 13%, respectively). We noted a consistent rise in particle delivery to the rod surface as the particle concentration in the suspension increased.

The particle adhesion is quantified by counting the loss of particles after each knot and the results are presented in Table 3. It can be observed that a higher number of particles adhered on the substrate as the binder concentration increases and their adhesion is stronger at higher binder concentration and hence relatively lower loss count can be observed. This trend can be attributed to the elevated binder concentration leading to an increase in polymer film thickness, subsequently enhancing the strength to retain particles in their desired locations.

The friction coefficient of the coated rod increases with the increase of the particle volume fraction in the suspension, which is shown in Fig. 8. It can be observed that the friction coefficient can be increased significantly with steep slope by coating the rod in only 1% irregular shaped particles. We also observed that the entrained

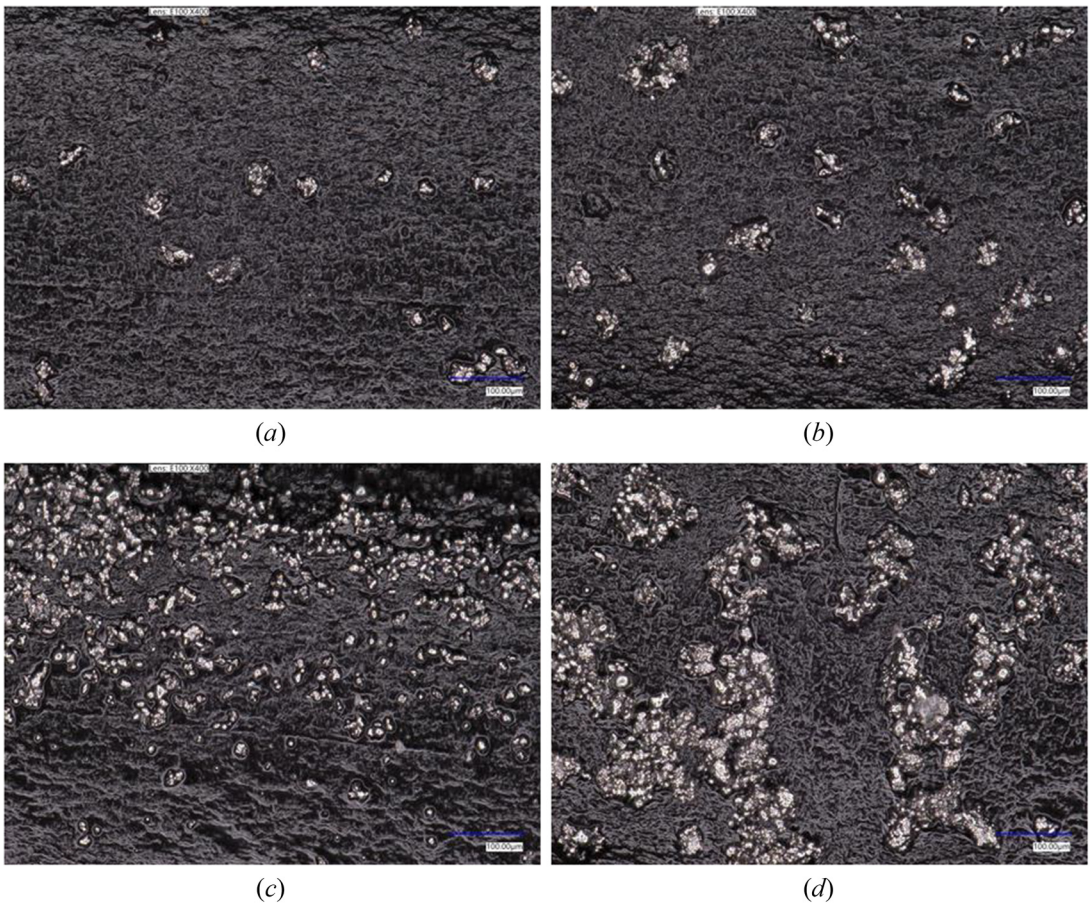

Fig. 7 Entrainment visualization of irregular particles: (*a*) 1% particle, (*b*) 4% particle, (*c*) 7% particle, and (*d*) 13% particle

Table 3 Variation of particle counts with binder concentration and knot experiments

Binder concentration (%)	Particles on coated rod, original (counts)	After one knot test		After two knot test		After three knot test	
		Particles remaining (counts)	Particle loss (%)	Particles remaining (counts)	Particle loss (%)	Particles remaining (counts)	Particle loss (%)
1	15 ± 10	11 ± 9	23	8 ± 8	43	7 ± 6	55
4	90 ± 43	66 ± 26	27	61 ± 25	32	51 ± 26	43
7	127 ± 30	113 ± 27	11	85 ± 21	33	60 ± 26	52
13	145 ± 24	130 ± 20	11	125 ± 16	14	95 ± 11	35

particles start to form clusters at 13%, which is the point of saturation for our experiment with irregular particles. Particle laden mixture start demonstrating non-Newtonian behavior at higher volume fraction (>10%), which has also been reported in literature [39]. Thus, the cluster formation at higher (13%) particle concentration can be attributed to this transition toward the complex mixture. To validate the findings about systematic variation of friction, two distinct systems are employed. The knot pull test serves as an indirect method for measuring the friction coefficient (μ) by gauging the friction force and subsequently calculating μ. In contrast, the capstan test provides a direct measurement of the friction coefficient for any flexible rods or ropes. The outcomes derived from the knot pull test are corroborated and validated through the results obtained from the capstan experiments.

The process discussed in this article is widely employed for transferring a diverse range of materials from solution, suspension, and mixture. Using cylindrical geometry is more representative of numerous applications (cables, wires, pipes, ropes, etc.) than flat substrates. Our surface treatment method is innovative as a scalable manufacturing process that could enable purposeful friction modifications. The particle transfer mechanism for tuning surface morphology distinguishes this work from prior adhesion or interface analyses. This specific coating method enables the evaluation of knot strength and the adjustment of the knot's strength, commonly known as the friction knob in the system. One competing method, spray coating, is commonly used for preparing thin films and facilitating particle transfer by controlling the properties of the suspension and the nozzle. Another rival technique for film preparation is spin coating, employed for forming thin films over a spinning substrate. Spin coating offers a more uniform distribution of particles, leading to improved coverage and uniformity in the resulting film. In contrast, the film thickness in dip coating is controlled by the withdrawal speed of the rod and the viscosity of the suspension. While both competing techniques are suitable for transferring nanomaterials, our approach has successfully demonstrated the transfer of microparticles from complex mixtures. However, creating homogeneous mixture or pseudo-suspension with the density mismatched microparticles can be challenging and may result in nonuniform particle transfer.

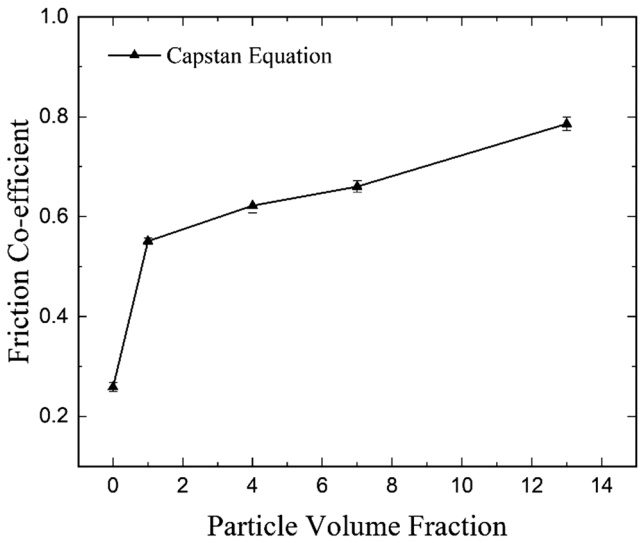

Fig. 8 Friction coefficient of the coated rod using capstan equation

4 Conclusion

The primary objective of this study is to demonstrate systematic control of the friction force on a smooth surface by introducing entrained particles across the surface of rods as asperities. To verify the systematic variation of friction, the knot performance has been selected as quantitative measure. Thus, elastic rubber rod is selected to coat with asperities to construct the overhand knot. In this study, using wet deposition-based particle delivery techniques, we demonstrate a rapid and cost-effective approach to modify the frictional characteristics of the rod surface. In the initial phase, a polymer coating was applied to the rods, yielding friction forces nearly identical to those observed on uncoated rods. Subsequently, we introduced spherical particles at varying concentrations to investigate the resultant changes in friction force. Notably, the utilization of irregularly shaped particles led to a substantial and noteworthy variation in both friction force and friction coefficient of the rods.

By incorporating particles into the LCS, we alter the surface roughness and create asperities that influence the friction forces during self-contact. By parameterizing the deposition process, we control particle coverage that can systematically tune the surface morphology of the rod's surface. The friction coefficient is then measured using the capstan equation, which allows for a quantitative assessment of the variation in friction forces. Our findings reveal the significant influence of particle size, shape, and concentration on the frictional behavior of the coated rods. As the particles adhere to the rod's surface, they introduce additional contact points, leading to changes in friction forces during self-contact. Different particle shapes exhibit distinct effects on the friction coefficient, with irregular or rough particles generally resulting in higher friction forces compared to smoother particles. Furthermore, the concentration of particles in the suspension plays a crucial role in determining the overall frictional behavior. Higher adherend irregular particle led to an increase in surface roughness, resulting in elevated friction forces.

This study provides valuable insights into the manipulation of friction forces on rods through particle deposition. The ability to control and modify frictional characteristics is of immense practical importance in various fields, including sports, manufacturing, and engineering. By understanding the underlying mechanisms and optimizing the particle deposition process, it becomes possible to tailor the frictional behavior of rods to specific applications. This research opens up new avenues for the design and development of advanced materials and technologies that rely on friction control for enhanced performance. A systematic study of the adherent force in entrained particle can be a future research direction.

Funding Data

- The National Science Foundation (Award Nos. CMMI-2101751 and CMMI-2101745; Funder ID: 10.13039/100000084).

Data Availability Statement

The datasets generated and supporting the findings of this article are obtainable from the corresponding author upon reasonable request.

References

[1] Kang, D. W., Kang, M., and Hahn, J. W., 2015, "Keystone Error Analysis of Projection Optics in a Maskless Lithography System," Int. J. Precis. Eng. Manuf., **16**(2), pp. 373–378.

[2] Lv, J.-T., Yan, Y., Zhang, W.-K., Liu, Y.-H., Jiang, Z.-Y., and Si, G.-Y., 2015, "Plasmonic Nanoantennae Fabricated by Focused Ion Beam Milling," Int. J. Precis. Eng. Manuf., **16**(4), pp. 851–855.

[3] Kobayashi, T., Bando, M., Kimura, N., Shimizu, K., Kadono, K., Umezu, N., Miyahara, K., et al., 2013, "Production of a 100-m-Long High-Quality Graphene Transparent Conductive Film by Roll-to-Roll Chemical Vapor Deposition and Transfer Process.," Appl. Phys. Lett., **102**(2), p. 023112.

[4] Chu, W.-S., Kim, C.-S., Lee, H.-T., Choi, J.-O., Park, J.-I., Song, J.-H., Jang, K.-H., and Ahn, S.-H., 2014, "Hybrid Manufacturing in Micro/Nano Scale: A Review," Int. J. Precis. Eng. Manuf.-Green Technol., **1**(1), pp. 75–92.

[5] Hong, Y.-S., Lee, S.-R., Kim, J.-H., and Lee, S.-Y., 2015, "Application of a DLC-Coating for Improving Hydrostatic Piston Shoe Bearing Performance Under Mixed Friction Conditions," Int. J. Precis. Eng. Manuf., **16**(2), pp. 335–341.

[6] Yang, Y., Kim, K.-H., and Ong, J. L., 2005, "A Review on Calcium Phosphate Coatings Produced Using a Sputtering Process—An Alternative to Plasma Spraying," Biomaterials, **26**(3), pp. 327–337.

[7] Hench, L. L., and West, J. K., 1990, "The Sol-Gel Process," Chem. Rev., **90**(1), pp. 33–72.

[8] Xiao, Y., Xu, Z., Liu, Y., Peng, L., Xi, J., Fang, B., Guo, F., Li, P., and Gao, C., 2017, "Sheet Collapsing Approach for Rubber-Like Graphene Papers," ACS Nano, **11**(8), pp. 8092–8102.

[9] Park, J., Shin, K., and Lee, C., 2014, "Optimized Design for Anti-Reflection Coating Process in Roll-to-Roll Slot-Die Coating System," Rob. Comput.-Integr. Manuf., **30**(5), pp. 432–441.

[10] Scriven, L., 1988, *Physics and Applications of Dip Coating and Spin Coating*, MRS Online Proceedings Library (OPL), New York, p. 121.

[11] Khoda, B., , A. M. M. N., Ahsan, and Shovon, S. M. N., 2021, "Dip Coating From Density Mismatching Mixture," ASME J. Micro Nano-Manuf., **9**(2), p. 021003.

[12] Rio, E., and Boulogne, F., 2017, *Withdrawing a Solid From a Bath: How Much Liquid is Coated*?, Elsevier, Amsterdam, The Netherlands, pp. 100–114.

[13] Ibrahim Khalil, M., Tong, D., Wang, G., Jawed, M. K., and Khoda, B., 2022, "Systematic Variation of Friction of Rods," ASME J. Appl. Mech., **89**(11), p. 111007.

[14] Tang, X., and Yan, X., 2017, "Dip-Coating for Fibrous Materials: Mechanism, Methods and Applications," J. Sol-Gel Sci. Technol., **81**(2), pp. 378–404.

[15] Galio, A. F., Lamaka, S. V., Zheludkevich, M. L., Dick, L. F. P., Müller, I. L., and Ferreira, M. G. S., 2010, "Inhibitor-Doped Sol–Gel Coatings for Corrosion Protection of Magnesium Alloy AZ31," Surf. Coat. Technol., **204**(9–10), pp. 1479–1486.

[16] Crosley, M. S., and Yip, W. T., 2018, "Kinetically Doped Silica Sol-Gel Optical Biosensors: Expanding Potential Through Dip-Coating," ACS Omega, **3**(7), pp. 7971–7978.

[17] Iijima, M., Muguruma, T., Brantley, W., Choe, H.-C., Nakagaki, S., Alapati, S. B., and Mizoguchi, I., 2012, "Effect of Coating on Properties of Esthetic Orthodontic Nickel-Titanium Wires," Angle Orthod., **82**(2), pp. 319–325.

[18] Murray, T. J., 2008, "Poly (Amide-Imides): Wire Enamels With Excellent Thermal and Chemical Properties," Macromol. Mater. Eng., **293**(5), pp. 350–360.

[19] Khalil, I., and Khoda, B., 2021, "Sorting of Poly-Disperse Particle by Entrapment Using Liquid Carrier System," ASME J. Manuf. Sci. Eng., **144**(5), p. 054502.

[20] Khalil, M. I., and Khoda, B., 2022, "Size-Based Filtration of Poly-Disperse Micro-Particle by Dipping," ASME Paper No. MSEC2022-85680.

[21] Dincau, B. M., Mai, E., Magdelaine, Q., Lee, J. A., Bazant, M. Z., and Sauret, A., 2020, "Entrainment of Particles During the Withdrawal of a Fibre From a Dilute Suspension," J. Fluid Mech., **903**, p. A38.

[22] Banerjee, S., and Mazumder, M. K., 1996, "Adhesion of Charged Powders on Metal Surface in Powder Coating Process," IEEE Trans. Ind. Appl., **32**(6), pp. 1243–1248.

[23] Dimitrov, A. S., and Nagayama, K., 1996, "Continuous Convective Assembling of Fine Particles Into Two-Dimensional Arrays on Solid Surfaces," Langmuir, **12**(5), pp. 1303–1311.

[24] Cong, H.-P., Chen, J.-F., and Yu, S.-H., 2014, "Graphene-Based Macroscopic Assemblies and Architectures: An Emerging Material System," Chem. Soc. Rev., **43**(21), pp. 7295–7325.

[25] Ness, C., Mari, R., and Cates, M. E., 2018, "Shaken and Stirred: Random Organization Reduces Viscosity and Dissipation in Granular Suspensions," Sci. Adv., **4**(3), p. eaar3296.

[26] Khoda, B., and Ahsan, A. M. M. N., 2021, "A Novel Rapid Manufacturing Process for Metal Lattice Structure," 3D Printing Addit. Manuf., **8**(2), pp. 111–125.

[27] Paulitsch, J., Schenkel, M., Schintlmeister, A., Hutter, H., and Mayrhofer, P. H., 2010, "Low Friction CrN/TiN Multilayer Coatings Prepared by a Hybrid High Power Impulse Magnetron Sputtering/DC Magnetron Sputtering Deposition Technique," Thin Solid Films, **518**(19), pp. 5553–5557.

[28] Lee, Y.-Z., and Jeong, K.-H., 1998, "Wear-Life Diagram of TiN-Coated Steels," Wear, **217**(2), pp. 175–181.

[29] Levich, B., and Landau, L., 1942, "Dragging of a Liquid by a Moving Plate," Acta Physicochim., **17**, p. 42.

[30] Deryagin, B., and Titievskaya, A., 1945, "Experimental Study of Liquid Film Thickness Left on a Solid Wall After Receding Meniscus," Dokl. Akad. Nauk USSR, **50**, pp. 307–310.

[31] Quéré, D., 1999, "Fluid Coating on a Fiber," Annu. Rev. Fluid Mech., **31**(1), pp. 347–384.

[32] White, D. A., and Tallmadge, J. A., 1966, "A Theory of Withdrawal of Cylinders From Liquid Baths," AIChE J., **12**(2), pp. 333–339.

[33] Shovon, S. M. N., Alam, A., Gramlich, W., and Khoda, B., 2022, "Micro-Particle Entrainment From Density Mismatched Liquid Carrier System," Sci. Rep., **12**(1), p. 9806.

[34] Khoda, B., Gramlich, W., Shovon, S. M. N., and Khalil, I., 2023, "Effect of Molecular Weight on Polymer Solution Facilitated Transfer of non-Brownian Particles," Prog. Org. Coat., **176**, p. 107394.

[35] Shovon, S. M. N., Khalil, I., Alam, A., and Khoda, B., 2022, "Effect of Withdrawal Velocity on Particle Entrainment From Density Mismatched Mixture," ASME Paper No. MSEC2022-85745.

[36] Colosqui, C. E., Morris, J. F., and Stone, H. A., 2013, "Hydrodynamically Driven Colloidal Assembly in Dip Coating," Phys. Rev. Lett., **110**(18), p. 188302.

[37] Sauret, A., Gans, A., Colnet, B., Saingier, G., Bazant, M. Z., and Dressaire, E., 2019, "Capillary Filtering of Particles During Dip Coating," Phys. Rev. Fluids, **4**(5), p. 054303.

[38] Bagheri, G. H., Bonadonna, C., Manzella, I., and Vonlanthen, P., 2015, "On the Characterization of Size and Shape of Irregular Particles," Powder Technol., **270**, pp. 141–153.

[39] Gans, A., Dressaire, E., Colnet, B., Saingier, G., Bazant, M. Z., and Sauret, A., 2019, "Dip-Coating of Suspensions," Soft Matter, **15**(2), pp. 252–261.